ELSEVIER

Aerospace Science and Technology 6 (2002) 283–294

Aerospace Science and Technology

www.elsevier.com/locate/aescte

GPS based prediction of the instantaneous impact point for sounding rockets

GPS gestützte Vorhersage des instantanen Auftreffpunktes für Höhenforschungsraketen

Oliver Montenbruck [a,*], Markus Markgraf [a], Wolfgang Jung [a], Barton Bull [b], Wolfgang Engler [c]

[a] *German Space Operations Center, Deutsches Zentrum für Luft- und Raumfahrt, DLR 82230 Weßling, Germany*
[b] *NASA, Goddard Space Flight Center, Wallops Flight Facility, Wallops Island, Virginia 23337-5099, USA*
[c] *Kayser-Threde GmbH, Wolfratshauser Staße 48, 81379 München, Germany*

Received 24 September 2001; received in revised form 20 February 2002; accepted 20 February 2002

Abstract

As part of the range safety operations during a sounding rocket launch, a real-time prediction of the instantaneous impact point (IIP) is performed to monitor the expected touch down point in case of a boost termination. Supplementary to traditional radar tracking, the IIP prediction is nowadays based on GPS navigation data, which offer an inherently higher accuracy and reduced data noise. To comply with the increased tracking performance, a consistent set of equations suitable for real-time computation of the approximate IIP is established. Aside from a consideration of gravitational forces, reference frame rotation and Earth curvature, the model can also account for drag during the ascent trajectory provided that a priori information on the ballistic properties of the launch vehicle is available. The algorithm is tested for a representative set of mission profiles and applied to GPS flight data of an Improved Orion rocket and a Maxus rocket launched at Esrange, Kiruna.

Zusammenfassung

Als Teil der Sicherheitsmassnahmen wird am Startplatz von Höhenforschungsraketen eine Echtzeit-Vorhersage des instantanen Auftreffpunktes (IIP) durchgeführt, um den zu erwartenden Ort des Aufschlags im Falle eines Schubabruchs zu überwachen. Ergänzend zu traditionellen Radarstationen wird die IIP Vorhersage heute mit Hilfe von GPS Navigationsdaten durchgeführt, die eine höhere inhärente Genauigkeit und ein niedrigeres Rauschen bieten. Um mit der gestiegenen Genauigkeit Schritt zu halten, wird im vorliegenden Beitrag ein konsistenter Satz von Gleichungen für die Echtzeitvorhersage des ungefähren Auftreffpunktes abgeleitet. Neben der Berücksichtigung der gravitativen Kräfte, der Rotation des Bezugssystems und der Erdkrümmung kann das Model auch die atmosphärische Abbremsung in der Aufstiegsphase berücksichtigen, falls entsprechende Informationen über die aerodynamischen Eigenschaften der Rakete verfügbar sind. Der Algorithmus wird anhand repräsentativer Missionsprofile getestet und auf echte GPS Flugdaten einer Improved Orion Rakete und der Maxus Rakete angewendet, die von Esrange, Kiruna, gestartet wurden.

Keywords: Instantaneous impact point; GPS; Sounding rockets

Schlüsselwörter: Instantaner Auftreffpunkt; GPS; Höhenforschungsraketen

1. Introduction

The instantaneous impact point (IIP) describes the touch-down point of a sounding rocket under the assumption of an immediate end of the propelled flight [5]. It is representative of a situation in which the rocket motor is instantaneously switched off by the mission control center following, e.g., a guidance error during the boost phase. The real-time computation and display of the IIP allows the range safety officer to discern whether the rocket would eventually land outside the permissible range area and thus necessitate an

* Corresponding author.
E-mail address: oliver.montenbruck@dlr.de (O. Montenbruck).

1270-9638/02/$ – see front matter
PII: S1270-9638(02)01163-X

abort of the boosted flight or even a destruction of the malfunctioning vehicle.

In view of the limited computing performance available in real-time data systems, simplified expressions for the forecast of the impact point are employed in common range safety facilities. Typically, a parabolic flight path in the local horizontal coordinate system is assumed, which is further corrected for Coriolis forces caused by the rotation of the reference frame with respect to inertial space. While the underlying simplifications are compatible with short flight times and are often barely discernible from radar based range and angle tracking, their limitations are immediately obvious for high-altitude sounding rockets tracked by GPS sensors.

GPS receivers derive the instantaneous location of the host vehicle as well as the current clock error from pseudorange measurements to a minimum of four (up to about 12) visible GPS satellites [4]. Likewise, the Cartesian velocity vector can be obtained from Doppler measurements or difference carrier phases. Representative raw data accuracies amount to 1 m (pseudorange), 1 $\mathrm{m\,s^{-1}}$ (Doppler), and 1 $\mathrm{cm\,s^{-1}}$ for differenced carrier phases. After the deactivation of the intentional GPS signal degradation (Selective Availability S/A), the final real-time positioning accuracy has increased from about 100 m to roughly 10 m and 1 $\mathrm{m\,s^{-1}}$ for typical single frequency receivers. Key error sources responsible for these performance limits comprise errors in the GPS broadcast ephemerides and ionospheric path delays. If necessary, further improvements can, however, be made by postprocessing raw measurements on ground using precise GPS ephemerides and total electron content measurements. The performance indices given above are likewise applicable for high dynamics applications, provided that necessary precautions have been taken to adapt the tracking loops and select adequate reference oscillators. Various suitable receivers have been developed by industry and research centers among which the Ashtech G12 HDMA has evolved as the most widely used model. The receiver provides navigation solutions at a rate of up to 10 Hz, which more than satisfies typical applications needs. The quoted tracking accuracies have been derived from laboratory tests using GPS signal simulators as well as real flights. Hardware-in-the loop tests using signal simulators allow a direct comparison of measured and simulated trajectories and can thus show the proper response of the receiver to the extreme signal dynamics involving high line-of-sight velocities, accelerations, and yerk (change of acceleration). Using 3rd order tracking loops and appropriate bandwidths the GPS signals can be tracked through the phases of high dynamics without loosing track or loosing the desired measurement accuracy. Despite the lack of a truth reference trajectory in real sounding rocket flights, supporting evidence for the quoted accuracies comes from differential GPS tracking with a ground based reference station [1], the comparison of tracking results obtained by different GPS receivers on the same flight [2], the self-consistency of position and velocity measurements (obtained by physically different tracking processes), the consistency of GPS derived acceleration profiles with accelerometer measurements and the consistency with dynamical trajectory models (during the free flight phase). Compared to individual tracking radars which suffer from a poor angle measurement accuracy, GPS tracking provides a clearly superior 3-dimensional navigation accuracy [7]. Even with elaborate trilateration systems and a $\sim$1 m ranging accuracy, the viewing geometry of the GPS constellation is generally more favorable giving a better position dilution of precision (PDOP) and an unobstructed visibility throughout the entire flight from launch to landing.

Following successful application in a variety of sounding rocket flights, GPS has recently been recommended as the baseline for range safety tracking systems both for cost and performance reasons [12] and is expected to provide the primary sensor for flight terminations systems in the near future. An effort has therefore been made to establish linearized expressions for the prediction of the instantaneous impact point that are accurate to the kilometer level over a range of representative sounding rockets mission profiles, yet simple enough to allow their real-time application. The quality of the derived model is compared against a Keplerian trajectory model with J_2 corrections which is shown to give precise IIP predictions in the absence of atmospheric drag but is computationally more involved than the linearized expressions.

At a given time t, we assume the GPS receiver to provide the instantaneous position $\mathbf{r}$ and velocity $\mathbf{v}$ of the rocket in the Earth-centered, Earth-fixed WGS84 system, or, alternatively, the WGS84 geodetic longitude λ, latitude φ, and altitude h as well as the ground speed u_{gnd}, flight azimuth (or heading) A, and the climb rate u_{up}. The two velocity representations are related to each other by the expression

$$\mathbf{v} = \mathbf{E}^{\mathrm{T}}(\lambda, \varphi) \cdot \mathbf{u}, \tag{1}$$

where the rows of $\mathbf{E}$ are the unit vectors $\mathbf{e}_{\mathrm{E}}$, $\mathbf{e}_{\mathrm{N}}$, and $\mathbf{e}_{\mathrm{up}}$ along the local East, North, and up direction and the vector

$$\mathbf{u} = \begin{pmatrix} u_{\mathrm{gnd}} \sin(A) \\ u_{\mathrm{gnd}} \cos(A) \\ u_{\mathrm{up}} \end{pmatrix} \tag{2}$$

denotes the velocity components along these axes. Expressions for the computation of $\mathbf{E}$ are given in standard text books, which likewise provide the classical relations for the conversion of Cartesian and geodetic positions (see, e.g., [4, 9]).

2. Linearized IIP model

In the sequel, linearized expressions for the closed-form computation of the instantaneous impact point are derived. Starting from a simple parabolic trajectory model, various corrections are made to account for the curvature of the surface of the Earth as well as the integral effects of the Coriolis force and gravity field changes along the trajectory.

Throughout the analysis, only first order corrections are considered, which limits the achievable accuracy of the expressions. Leading error terms in the resulting model are caused by the neglect of Coriolis force changes due to gravity field variations along the trajectory as well as the neglect of second order terms in the altitude dependence of the gravity field. Despite these restrictions the resulting model is more complete and of higher accuracy than conventional IIP algorithms based on a flat Earth approximation with Coriolis correction (see, e.g., [13]).

2.1. Parabolic flight

To lowest order, the trajectory of a sounding rocket is represented by a parabolic motion under the action of a constant acceleration $\ddot{h} = -g$ along the local vertical. Making use of a local horizontal coordinate system which is aligned with the instantaneous East, North, and up direction and originates in the foot point of the satellite at time t_0 (cf. Fig. 1), the subsequent flight path is described by the quadratic equation

$$\begin{aligned}\mathbf{s}(t_0+\Delta t) &= \mathbf{s}_0 + \mathbf{u}_0\Delta t + \frac{1}{2}\mathbf{g}\Delta t^2 \\ &= \begin{pmatrix}0\\0\\h_0\end{pmatrix} + \begin{pmatrix}u_{0,\mathrm{E}}\\u_{0,\mathrm{N}}\\u_{0,\mathrm{up}}\end{pmatrix}\Delta t + \frac{1}{2}\begin{pmatrix}0\\0\\-g\end{pmatrix}\Delta t^2. \end{aligned} \quad (3)$$

Upon equating the vertical component to zero, the time after which the rocket crosses the horizontal plane is obtained as

$$\tau = \frac{1}{g}\left(u_{0,\mathrm{up}} + \sqrt{u_{0,\mathrm{up}}^2 + 2h_0 g}\right) \quad (4)$$

and the resulting impact point in the global WGS84 reference system is given by

$$\begin{aligned}\mathbf{r}_{\mathrm{IIP}}(t_0) &= \mathbf{r}(t_0) + \mathbf{E}^{\mathrm{T}}(t_0)(\mathbf{s}(t_0+\tau) - \mathbf{s}_0) \\ &= \mathbf{r}_0(t) + \mathbf{E}^{\mathrm{T}}(t)\begin{pmatrix}u_{0,\mathrm{E}}\tau\\u_{0,\mathrm{N}}\tau\\-h\end{pmatrix}. \end{aligned} \quad (5)$$

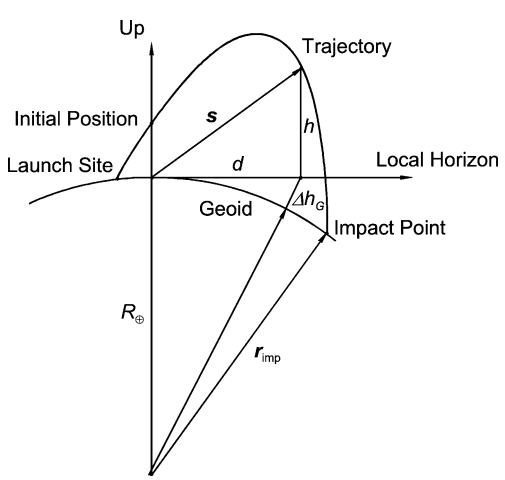

Fig. 1. Geometry of sounding rocket trajectory for instantaneous impact point prediction.

For completeness, we also provide the magnitude

$$u_{\mathrm{imp}} = |\dot{h}(t_0+\tau)| = -(u_{0,\mathrm{up}} - g\tau) \quad (6)$$

of the vertical impact velocity, which is repeatedly required in the subsequent discussion.

2.2. Surface gravity

Neglecting higher order terms, the effective acceleration experienced by the rocket in the local horizontal system is the sum of the Earth's central attraction, the centrifugal force and the J_2 perturbation. Since the WGS84 reference ellipsoid that defines the local horizon system represents an equipotential surface, the resulting force vector is always perpendicular to the ground plane. Given the Earth's gravitational coefficient $GM_\oplus$, the equatorial radius $R_\oplus$, the angular velocity $\omega_\oplus$, the flattening f and the gravity field coefficient $J_2 = -C_{20}$, one obtains the expression

$$\begin{aligned} g_{\mathrm{eff}} &= \frac{GM_\oplus}{R_\oplus}\left(1 - \frac{\omega_\oplus^2 R_\oplus^3}{GM_\oplus} + \frac{3}{2}J_2\right) \\ &\quad + \frac{GM_\oplus}{R_\oplus}\left(2f + \frac{\omega_\oplus^2 R_\oplus^3}{GM_\oplus} - \frac{9}{2}J_2\right)\sin^2(\varphi) \end{aligned} \quad (7)$$

or

$$g_{\mathrm{eff}} = 9.7803\,\mathrm{m\,s^{-2}}\left(1 + 0.005279\sin^2(\varphi)\right). \quad (8)$$

[11] for the sum of the vertical components of the central, centrifugal and J_2 attraction.

2.3. Earth curvature

With increasing flight distance, the local horizontal plane deviates quadratically from the geoid and is thus no longer a suitable reference for the IIP prediction. Assuming a spherical Earth of radius $R_\oplus$, a point on the horizon at a distance d has an altitude of

$$\Delta h_G = R_\oplus\left(1/\cos(\arctan(d/R_\oplus)) - 1\right) \approx \frac{1}{2}\frac{d^2}{R_\oplus} \quad (9)$$

above the geoid (Fig. 1). This yields a correction

$$\Delta h_G = \frac{(u_{0,\mathrm{E}}^2 + u_{0,\mathrm{N}}^2)}{2R_\oplus}\tau^2 \quad (10)$$

of the vertical IIP component of the IIP, which amounts to 0.5 km at a ground range of 80 km. At the same time, the flight time is increased by an amount $\delta\tau = \Delta h_G/u_{\mathrm{imp}}$, which results in an associated change of the ground range. The total IIP correction is thus obtained as

$$\Delta\mathbf{r}_{\mathrm{IIP}}(t_0) = \mathbf{E}^{\mathrm{T}}(t_0)\frac{(u_{0,\mathrm{E}}^2 + u_{0,\mathrm{N}}^2)\tau^2}{2R_\oplus}\begin{pmatrix}u_{0,\mathrm{E}}/u_{\mathrm{imp}}\\u_{0,\mathrm{N}}/u_{\mathrm{imp}}\\-1\end{pmatrix}. \quad (11)$$

2.4. Coriolis force

The motion in the local horizontal coordinate system is subject to apparent forces resulting from the rotation of the Earth with respect to the inertial space. While the centrifugal force has already been accounted for in the effective vertical acceleration, the Coriolis force introduces an additional acceleration

$$\Delta\dot{\mathbf{u}} = 2\mathbf{u} \times \boldsymbol{\omega} \tag{12}$$

[6] into the equation of motion, where

$$\boldsymbol{\omega} = \begin{pmatrix} 0 \\ \omega_\oplus \cos(\varphi) \\ \omega_\oplus \sin(\varphi) \end{pmatrix} \tag{13}$$

denotes the East, North, and up components of the Earth's angular velocity vector. Inserting the unperturbed velocity into the right-hand side of (12) yields the expression

$$\begin{aligned} \Delta\dot{\mathbf{u}}(t_0 + \Delta t) &= 2(\mathbf{u}_0 + \mathbf{g}\Delta t) \times \boldsymbol{\omega} \\ &= 2(\mathbf{u}_0 \times \boldsymbol{\omega}) + 2(\mathbf{g} \times \boldsymbol{\omega})\Delta t, \end{aligned} \tag{14}$$

which may be integrated twice to obtain the resulting Coriolis correction

$$\begin{aligned} \Delta\mathbf{s}(t_0 + \Delta t) &= (\mathbf{u}_0 \times \boldsymbol{\omega})\Delta t^2 + \frac{1}{3}(\mathbf{g} \times \boldsymbol{\omega})\Delta t^3 \\ &= \omega_\oplus \begin{pmatrix} +u_{0,\mathrm{N}} \sin(\varphi) - u_{0,\mathrm{up}} \cos(\varphi) \\ -u_{0,\mathrm{E}} \sin(\varphi) \\ +u_{0,\mathrm{E}} \cos(\varphi) \end{pmatrix} \cdot \Delta t^2 \\ &\quad + \frac{1}{3}\omega_\oplus g \begin{pmatrix} +\cos(\varphi) \\ 0 \\ 0 \end{pmatrix} \cdot \Delta t^3 \end{aligned} \tag{15}$$

of the rocket position at a time Δt after the current epoch t_0. While the East and North component of the above expression translate directly into a corresponding correction of the predicted impact point coordinates, the vertical component implies an increment $\delta\tau = \omega_\oplus u_{0,\mathrm{E}} \cos(\varphi)\tau^2/u_{\mathrm{imp}}$ to the computed flight time and an associated extension of the ground track. As a result, the total IIP correction for Coriolis forces is given by the expression

$$\begin{aligned} &\Delta\mathbf{r}_{\mathrm{IIP}}(t_0) \\ &= \mathbf{E}^{\mathrm{T}}(t_0) \left[\omega_\oplus \begin{pmatrix} +u_{0,\mathrm{N}} \sin\varphi + (u_{0,\mathrm{E}}^2/u_{\mathrm{imp}} - u_{0,\mathrm{up}}) \cos\varphi \\ -u_{0,\mathrm{E}} \sin\varphi + (u_{0,\mathrm{N}} u_{0,\mathrm{E}}/u_{\mathrm{imp}}) \cos\varphi \\ 0 \end{pmatrix} \right. \\ &\quad \left. \cdot \tau^2 + \frac{\omega_\oplus g}{3} \begin{pmatrix} \cos\varphi \\ 0 \\ 0 \end{pmatrix} \cdot \tau^3 \right]. \end{aligned} \tag{16}$$

It is noted that the indirect Coriolis correction caused by the change in flight time is only relevant for a rocket launched in an eastern or western direction, whereas it has no effect for northbound or southbound trajectories.

2.5. Gravity field variation

The assumption of a constant gravitational acceleration made in Section 2.1 is clearly violated when the sounding rocket achieves an altitude or ground range that is no longer small compared to the radius of the Earth.

While the vector of the gravitational acceleration is always perpendicular to the surface of the geoid, the same does not apply for the local horizontal coordinate system used to describe the flight path between the current rocket location and the impact point. The plumb line coincides with the up-axis at the initial epoch t_0, but is subsequently deflected by an angle

$$\psi \approx \arctan(d/R_\oplus) \approx d/R_\oplus \tag{17}$$

that roughly matches the geocentric angle between the foot points at times t_0 and t and increases in proportion to the ground separation d (Fig. 1). As a result, the rocket experiences a horizontal acceleration of magnitude $g \cdot \sin(\psi)$ in anti-flight direction which reduces the ground speed and thus the IIP distance. Using the unperturbed flight path (3) as a first approximation, the perturbational acceleration caused by the deflection of the gravity field vector can be expressed as

$$\Delta\ddot{\mathbf{s}}(t_0 + \Delta t) = -\frac{g}{R_\oplus} \begin{pmatrix} u_{0,\mathrm{E}} \\ u_{0,\mathrm{N}} \\ 0 \end{pmatrix} \Delta t. \tag{18}$$

Upon double integration this yields an accumulated correction

$$\Delta\mathbf{r}_{\mathrm{IIP}}(t_0) = \mathbf{E}^{\mathrm{T}}(t_0) \left[-\frac{g}{6R_\oplus} \begin{pmatrix} u_{0,\mathrm{E}} \\ u_{0,\mathrm{N}} \\ 0 \end{pmatrix} \tau^3 \right] \tag{19}$$

to the predicted IIP.

In addition to the varying orientation of the plumb line, the magnitude of the gravitational acceleration changes with the inverse square of the sounding rocket's distance from the geocenter. For sufficiently small altitudes h, the change of the gravitational acceleration with respect to the surface value can be described by the linearized expression

$$\Delta g(h) \approx \frac{\partial}{\partial h} \left(g \frac{R_\oplus^2}{(R_\oplus + h)^2} \right) h = -\frac{2gh}{R_\oplus}, \tag{20}$$

which yields the differential equation

$$\Delta\ddot{h} = \frac{2g}{R_\oplus} h(t) \approx \frac{2g}{R_\oplus} \left(h_0 + u_{0,\mathrm{up}}\Delta t - \frac{1}{2} g \Delta t^2 \right) \tag{21}$$

for the corresponding altitude correction. Double integration then yields the relation

$$\Delta h(\tau) = \frac{g}{R_\oplus} \tau^2 \left(h_0 + \frac{1}{3} u_{0,\mathrm{up}} \tau - \frac{g}{12} \tau^2 \right), \tag{22}$$

which may further be expressed as

$$\Delta h(\tau) = \frac{1}{3R_\oplus} (h_0 + u_{0,\mathrm{up}}\tau)(5h_0 + u_{0,\mathrm{up}}\tau) \tag{23}$$

by considering the identity $2(h_0 + u_{0,\mathrm{up}}\tau) = g\tau^2$ derived from the condition of a vanishing impact point altitude. Again, the correction of the rocket altitude increases the time to impact by an amount $\delta\tau = \Delta h/u_{\mathrm{imp}}$, and the location of the impact point is in turn shifted by

$$\Delta\mathbf{r}_{\mathrm{IIP}}(t_0) = \mathbf{E}^{\mathrm{T}}(t_0)\left[\frac{1}{3R_\oplus}\frac{(h_0+u_{0,\mathrm{up}}\tau)(5h_0+u_{0,\mathrm{up}}\tau)}{u_{\mathrm{imp}}}\begin{pmatrix}u_{0,\mathrm{E}}\\ u_{0,\mathrm{N}}\\ 0\end{pmatrix}\right]. \tag{24}$$

It may be observed that the tilt of the gravity vector reduces the IIP distance while the reduction of the gravity acceleration with altitude increases the total flight time and thus the IIP range. Some level of cancellation therefore exists, which explains the reasonable accuracy of IIP predictions assuming a constant gravitational acceleration along the vertical. The exact balance does, however, depend on the actual flight profile and it is therefore advisable to always include the respective corrections. Furthermore, we note that the Taylor expansion of the gravitational field strength involves notable second order terms for altitudes of about 10% of the Earth radius and above. This is well within the range of common sounding rockets and places a natural limit to the quality of the linearized IIP prediction model.

3. Applications

To assess the quality of the linearized IIP prediction model, various applications are considered in the sequel. The set of test cases comprises the launch of an Improved Orion rocket and a Maxus rocket from Esrange, Kiruna, as well as the launch of a VS40 rocket from Alcantara, Brazil. As illustrated in Table 1, the three scenarios cover a wide spectrum of flight parameters and may thus be considered as representative for other missions within the covered range of altitudes and ground ranges.

While the VS40 trajectory is based on a ground simulation, actual GPS measurements are employed for the impact point prediction of the Improved Orion and Maxus rockets. In both cases the navigation solutions have been obtained by Asthech G12 HDMA receivers released for use outside the regular DOD limitations. While an absolute accuracy assessment is hard to obtain in the absence of a superior and independent tracking system, the G12 position and velocity measurements are generally consistent to the level of 10 m and 1 m/s, respectively, with data collected by other GPS receivers on the same flights [2,8,10].

In all test cases, the measured (or simulated) trajectory data were consistently expressed as Cartesian position and velocity in the WGS84 system, which represents the native form of the navigation solution inside a GPS receiver. Using 1 s samples of these data, the WGS84 coordinates of the instantaneous impact point were then predicted for the entire flight and finally converted into the local horizontal coordinate system of the launch site to facilitate representation of the results.

As a reference for the evaluation of the linearized IIP model, impact point predictions have, furthermore, been obtained from a perturbed Keplerian trajectory model. To this end, the state vector was first transformed into an inertial reference system before computing the Keplerian elements of an osculating ellipse. By iteration, the intersection of the elliptic orbit with the reference ellipsoid was then determined and the resulting impact point was finally expressed in the WGS84 system by considering the Earth rotation during the remaining flight time. To account for perturbations caused by Earth oblateness, the acceleration $\mathbf{a}_{J2}$ due to the first zonal harmonic of the Earth's gravity field has, furthermore, been computed at the instantaneous location $\mathbf{r}(t_0)$ and used to obtain a first order correction

$$\Delta\mathbf{r}_{J2}(t_0) = \frac{1}{2}\mathbf{a}_{J2}\tau^2, \tag{25}$$

which was applied to the Keplerian orbit prediction prior to the iteration of the impact point location. Here τ denotes the parabolic flight time obtained from (4) with a mean value $g = 9.81\ \mathrm{m\,s^{-2}}$ of the gravitational acceleration. While the resulting model likewise neglects any perturbations caused by atmospheric drag during the ascent or reentry, it provides an accurate modeling of the shape of the Earth, the central gravitational force and the reference frame rotation irrespective of the achieved altitude, ground range and flight time.

Table 1
Approximate flight parameters for Improved Orion (Test Maxus-4 campaign), Maxus-4 and VS40 scenario

Parameter	Test Maxus-4	Maxus-4	VS40
Launch site	$\lambda = +21.1°$, $\varphi = +67.9°$	$\lambda = +21.1°$, $\varphi = +67.9°$	$\lambda = -44.4°$, $\varphi = -2.3°$
Boost duration (1st stage)	6 s	65 s	62 s
Boost duration (2nd stage)	25 s	n.a.	71 s
Flight time (to parachute)	370 s	940 s	ca. 900 s
Apogee altitude	80 km	700 km	660 km
Horizontal range	65 km	95 km	780 km
Max. velocity	1100 $\mathrm{m\,s^{-1}}$	3300 $\mathrm{m\,s^{-1}}$	3200 $\mathrm{m\,s^{-1}}$
Max. acceleration	18 g	13 g	6.4 g

3.1. Improved Orion trajectory

Within the Test Maxus-4 campaign, an Improved Orion rocket was launched from Esrange, Kiruna on 19 Feb. 2001 to validate the relevant range safety systems for the upcoming Maxus-4 mission. The rocket achieved an apogee altitude of 80 km after a flight time of $2^{m}17^{s}$ and performed the reentry at a ground distance of roughly 65 km from the launch site. GPS tracking data were collected by a total of three receivers, out of which the Ashtech G12 HDMA operated by NASA/WFF provided the best accuracy and overall coverage [2,3,8].

Results of the IIP prediction for the Test Maxus-4 flight are illustrated in Fig. 2. The first and second boost phase of the Improved Orion rocket are readily distinguished from the changing separation between subsequent impact point predictions that are always separated by a one second time interval. After burn-out of the second stage ($t = 25$ s), which takes place at an altitude of only 20 km, a maximum IIP range of 72 km is predicted. Thereafter, the IIP moves back south till $t = 50$ s, at which time a stable location 66.5 km north and 8 km west of the launch site is achieved. The rapid change in the computed impact point is clearly caused by residual atmospheric drag between burn-out and an altitude of about 45 km, which is not accounted for in any of the employed IIP prediction models. Similarly, the computed IIP starts to spiral away from the stable point as the payload enters the atmosphere again at the end of the free flight phase ($t = 230$ s, $h = 41$ km) and starts an erratic tumbling motion down to the parachute release. In total the IIP moves by roughly 5 km during the atmospheric reentry. Low altitude winds finally cause a south-east drift of the payload and the impact point by another 5 km prior to touch down.

As implied by the moderate altitude and ground range of the Improved Orion rocket, the approximations in the linearized IIP model are well justified for the Test Maxus-4 flight and the predictions differ only negligibly from those of the perturbed Keplerian model (Table 2). Even a simple parabolic model with a mean value $g = 9.81\ \mathrm{m\,s^{-2}}$ of the gravitational acceleration yields competitive results and the biggest IIP corrections amount to less than 1 km in total. Despite the excellent modeling of the free flight trajectory, it is evident, however, that atmospheric perturbations pose a natural limit to the IIP prediction accuracy. This is particularly true for the reentry and atmospheric descent, where the translational and rotational dynamics of the rocket are closely coupled and too complex to allow a deterministic modeling.

3.2. Maxus-4 mission

The Maxus-4 mission was conducted at Esrange, Kiruna, on April 29, 2001 and comprised seven material sciences experiments in five different experiment units. A single stage Castor-4B motor carried the payload to an altitude of 703.4 km and allowed for a zero-g time of more than twelve

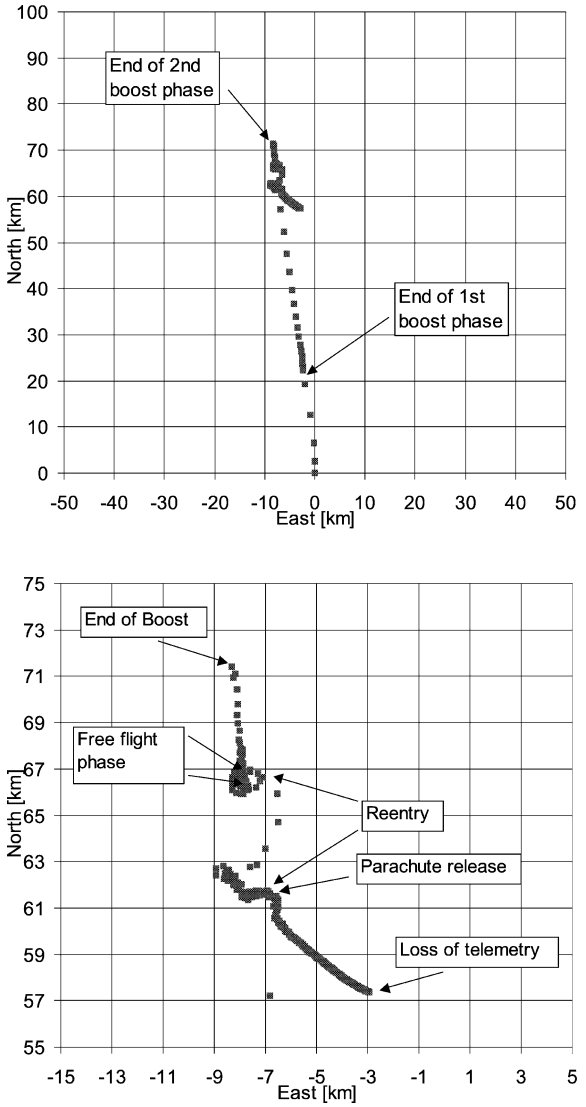

Fig. 2. GPS based instantaneous impact point prediction for the Improved Orion rocket flown within the Test Maxus-4 campaign. The impact point coordinates are referred to a local horizontal coordinate system originating at the launch site and apply for the linearized IIP model. Within the resolution of the graph, matching results are obtained for the perturbed Keplerian model.

minutes. Due to problems in the guidance system, the flight path started to deviate from the planned trajectory from about 10 s after lift-off. As a result, the ground track was shifted in a westerly direction and the payload ultimately crossed the border before landing in Norway. Furthermore, the main parachute was destroyed after being deployed too early due to a malfunction, which resulted in a final sink rate of about $90\ \mathrm{m\,s^{-1}}$.

As part of the Kayser-Threde service module an Ashtech G12 HDMA receiver was used to track the Maxus-4 payload and provide GPS navigation data for an operational IIP prediction. Due to restrictions of the available antenna system no GPS tracking was possible from start of reentry up the parachute release and the G12 receiver failed to reacquire

Table 2
Instantaneous impact point prediction for the Improved Orion rocket flown in Test-Maxus-4 mission. All coordinates refer to the local horizontal system of the launch site. Offsets are given with respect to the IIP predicted prior to the atmospheric reentry

Time since lift-off [s]	Model	IIP [km]			Offset [km]		
		East	North	Up	East	North	Up
25 s (Post boost)	Kepler + $J2$	−8.290	71.369	−0.755	−0.320	4.865	−0.054
50 s	”	−7.836	66.789	−0.704	0.134	0.285	−0.003
230 s (Start reentry)	”	−7.970	66.504	−0.701	0.000	0.000	0.000
370 s (Parachute release)	”	−6.659	61.413	−0.650	1.311	−5.091	0.051
820 s (Loss of telemetry)	”	−2.916	57.360	−0.610	5.054	−9.144	0.091
50 s	Parabolic ($g = 9.81$)	−8.444	66.404	−0.454	−0.474	−0.100	0.247
50 s	Parabolic + corrections	−7.880	66.738	−0.702	0.090	0.234	−0.001
IIP corrections of linearized model (at $t_0 = 50$ s)		East	North	Up			
Gravity (flattening, centrifugal force, $J2$)		0.008	−0.068	0.000			
Geoid shape		−0.006	0.050	−0.247			
Coriolis force		0.626	0.096	0.000			
Gravity (deflection, altitude variation)		−0.064	0.256	−0.001			

satellites prior to the impact. The subsequent analysis has therefore been supplemented by navigation data obtained from an experimental Orion GPS receiver that was flown on the same module [10]. While the Orion GPS data exhibit a temporarily degraded performance in response to a high yerk at boost end, they do cover the final mission phase from parachute release to loss of touchdown and thus add valuable information for the assessment of the IIP prediction.

For completeness, we also mention that the G12 data collected during the Maxus-4 mission have been corrected for an inconsistency of position and velocity data in the XF02 receiver software version that became apparent during the data analysis and was independently confirmed by the manufacturer. While the position data bear a proper time tag, the velocity data within a navigation record refer to an instant of 0.25 s earlier than the given time stamp. Using linear extrapolation, the position data were, therefore, referred to the same time as the velocity data and the time tag was modified accordingly.

Results of the IIP prediction for the Maxus-4 flight are illustrated in Fig. 3, which clearly shows the off-nominal evolution of the predicted impact point caused by problems of the guidance system. The operational real-time IIP prediction carried out at Esrange during the Maxus-4 flight based on GPS telemetry (Viertotak, priv. comm.) closely matches the results obtained within the present analysis. Some systematic excursions may, however, be observed, which are evidently caused by an improper conversion of the GPS velocity data into the reference frame of the impact point prediction. For completeness we note that the radar based IIP prediction was found to be too noisy to allow a reliable assessment of the impact region. GPS data provided sufficient evidence for only a minor violation of the range safety boundary which ultimately avoided the need to destroy the rocket during the boost phase.

A close look at the evolution of the IIP during the parabolic free flight phase clearly reveals the performance differences between the more rigorous perturbed Keplerian

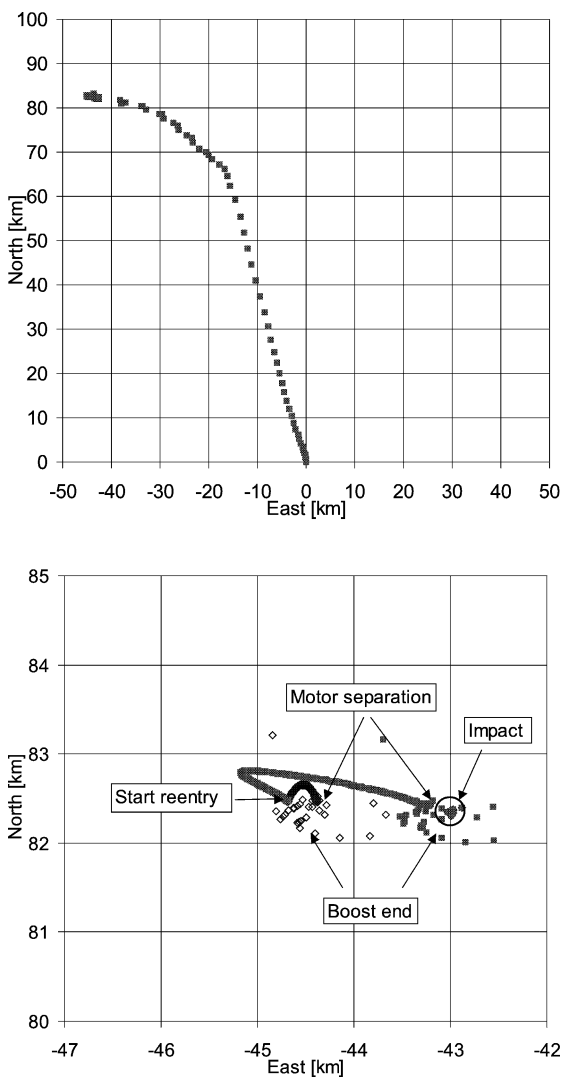

Fig. 3. GPS based IIP prediction for the Maxus-4 sounding rocket in the Esrange launcher coordinate system. Predictions obtained by the linearized IIP model are shown as solid squares, while the reference solution based on the perturbed Keplerian model is indicated by open diamonds.

Table 3
Instantaneous impact point prediction for the Maxus-4 flight. All coordinates refer to the local horizontal system of the launch site. Offsets are given with respect to the IIP predicted prior to the atmospheric reentry

Time since lift-off [s]	Model	IIP [km]			Offset [km]		
		East	North	Up	East	North	Up
100 s	Kepler + $J2$	−44.390	82.467	−1.037	0.288	−0.023	0.002
850 s (Start reentry)	”	−44.678	82.490	−1.039	0.000	0.000	0.000
960 s (Loss of telemetry)	”	−42.989	82.307	−1.026	1.689	−0.183	0.013
100 s	Parabolic ($g = 9.81$)	−36.027	79.166	−0.498	8.651	−3.324	0.541
100 s	Parabolic + corrections	−43.276	82.423	−0.952	1.402	−0.067	0.087
IIP corrections of linearized model (at $t_0 = 100$ s)		East	North	Up			
Gravity (flattening, centrifugal force, $J2$)		0.043	−0.092	0.000			
Geoid shape		−0.006	0.012	−0.444			
Coriolis force		−6.388	1.433	−0.006			
Gravity (deflection, altitude variation)		−0.898	1.904	−0.004			

model and the linearized IIP model developed in the previous section. While the former model yields self-consistent IIP predictions within a level of a few hundreds of meters during the entire micro-gravity phase, the simplified model exhibits a systematic wander of the IIP by roughly 2 km between motor separation and start of the atmospheric reentry. In view of the extended flight time and the achieved apogee height, the results nevertheless demonstrate the high quality of the latter model. During the atmospheric reentry no GPS tracking data could be collected due to the lack of a suitable antenna. Right after parachute release, a short set of position and velocity measurements could, however, be obtained before the loss of telemetry and the final impact. As shown in Fig. 3, the actual impact point differs by only 2 km from the forecast obtained up to the start of reentry. Evidently, the atmospheric perturbations during reentry were considerably less pronounced in the Maxus-4 mission than in the previously discussed flight of the Improved Orion sounding rocket.

More detailed information on the obtained impact point predictions is collated in Table 3. Clearly a simple parabolic model is inadequate for the given trajectory and Coriolis forces as well as changes of the gravity field during the flight have to be accounted for. The associated corrections amount to 6.5 km and 2.1 km, respectively, where the latter term results from a near cancellation of the IIP shifts due an increased flight time (cf. (24); 10.5 km) and the deflection of the gravity field vector (cf. (19); 8.5 km).

3.3. VS40 scenario

The Brazilian VS40 is a dual stage rocket, which is launched from Alcantara Space Center and achieves a maximum altitude of 660 km at an assumed payload mass of 477 kg [14]. The scenario provides a valuable complement to the test cases discussed above, since it refers to a near equatorial launch site with a north-eastern flight direction and achieves a much larger ground range.

As shown in Fig. 4 and Table 4, the simplifications of the linearized model introduces peak errors of about 5 km, while

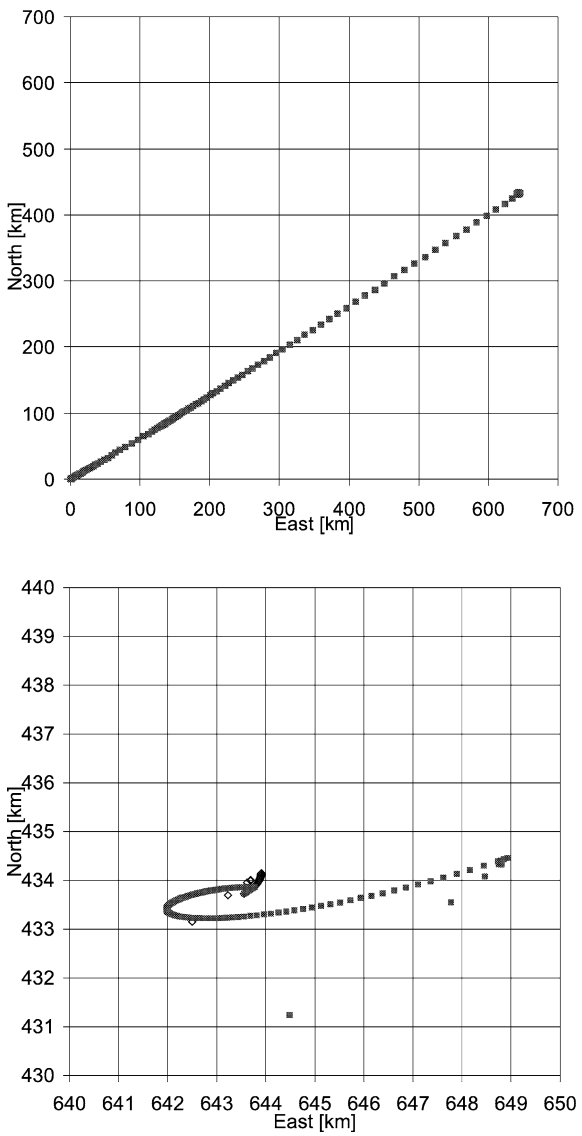

Fig. 4. Instantaneous impact point prediction for the simulated VS40 scenario. Predictions obtained by the linearized IIP model are shown as solid squares, while the reference solution based on the perturbed Keplerian model is indicated by open diamonds. Coordinates refer to the local horizontal system originating in the launch site.

Table 4
Instantaneous impact point prediction for the simulated VS40 trajectory. All coordinates refer to the local horizontal system of the launch site. Offsets are given with respect to the IIP predicted prior to the atmospheric reentry

Time since lift-off [s]	Model	IIP [km]			Offset [km]		
		East	North	Up	East	North	Up
150 s	Kepler + $J2$	643.682	433.998	−47.596	0.127	0.274	−0.031
910 s (Start reentry)	”	643.555	433.724	−47.565	0.000	0.000	0.000
150 s	Parabolic ($g = 9.81$)	634.319	410.625	−8.198	−9.236	−23.099	39.367
150 s	Parabolic + corrections	648.809	434.346	−45.341	5.254	0.622	2.224
IIP corrections of linearized model (at $t_0 = 100$ s)		East	North	Up			
Gravity (flattening, centrifugal force, $J2$)		1.583	1.028	−0.021			
Geoid shape		9.553	6.216	−36.991			
Coriolis force		−13.520	5.513	0.096			
Gravity (deflection, altitude variation)		16.874	10.964	−0.227			

the errors of a simple parabolic model are about five times higher. Individual corrections applied in the linearized IIP model amount to 15 km (Coriolis force) and 20 km (Gravity) but partially cancel each other in the East direction.

4. Atmospheric drag

The limited performance of both the perturbed Keplerian model and the linearized IIP prediction model for the Test Maxus-4 case motivates a more detailed discussion of atmospheric forces on the sounding rocket trajectory. Clearly, the associated perturbations are most pronounced in the dense part of the atmosphere and are thus confined to the early ascent phase and the final descent of the rocket or payload. In representative sounding rocket missions, the latter phase is characterized by an unstable, tumbling motion which renders an accurate dynamical modeling virtually impossible. This is well illustrated by both the pronounced lateral accelerations encountered during the Test Maxus-4 reentry and notable variations in the effective area-to-mass ratio that can be deduced from the observed along-track deceleration. The ascent phase of a sounding rocket, on the other hand, is readily described by common drag models in view of a stable attitude maintained by either passive or active control.

Following [13] the atmospheric density in the lower altitude regime ($h < 120$ km) can well be described by an exponential model

$$\rho(h) = \rho_0 \mathrm{e}^{-h/H} \tag{26}$$

despite existing temperature variations in the concerned layers. Here, the two parameters $H = 6.7$ km and $\rho_0 = 1.752\ \mathrm{kg\,m^{-3}}$ denote the atmospheric scale height and the density at ground as determined from a fit to actual densities over the altitude range of interest. The resistance of the atmosphere gives rise to an acceleration (drag) along the anti-velocity vector, which is described by the relation

$$\dot{\mathbf{u}} = -\left(\frac{\rho}{2\beta}\right) u\mathbf{u}, \tag{27}$$

where the ballistic coefficient

$$\beta = \frac{m}{C_\mathrm{D} A}, \tag{28}$$

denotes the ratio of mass and effective cross-section. For the Test Maxus-4 rocket (including motor and payload with a total mass of 528.4 kg), a value of $\beta = 7000\ \mathrm{kg\,m^{-2}}$ has been determined from the observed non-gravitational acceleration after the end of the boost phase.

When incorporated into a numerical integration of the equation of motion, the above drag model provides an accurate representation of the Test Maxus-4 trajectory from burn-out up to an altitude of roughly 45 km, where drag becomes small enough to be neglected in the IIP prediction. To avoid the burden and complexity of a numerical trajectory model it is again desirable, however, to obtain simplified expressions that directly relate the change in IIP position to the ballistic coefficient and the current orbital parameters.

In the sequel, a coarse correction to the drag-free IIP is, therefore, derived by modeling the accumulated deceleration during the ascent trajectory as an impulsive velocity decrement along the instantaneous flight direction. Based on the total differential of the impact condition

$$h_0 + u_{0,\mathrm{up}}\tau - \frac{1}{2} g\tau^2 = 0 \tag{29}$$

we may first relate the change

$$\begin{aligned} \Delta\tau &= \frac{\tau}{u_{0,\mathrm{up}} - g\tau}\Delta u_{0,\mathrm{up}} = \frac{\tau}{u_{0,\mathrm{imp}}}\Delta u_{0,\mathrm{up}} \\ &= \frac{\tau}{u_{0,\mathrm{imp}}} u_{0,\mathrm{up}}\left(\frac{\Delta u}{u}\right) \end{aligned} \tag{30}$$

in flight time to a change Δu of the total velocity u at the instantaneous altitude. Aside from the vertical velocity component, the ground velocity component is also changed in proportion to $\Delta u/u$, which gives rise to a total change

$$\begin{aligned} d\mathbf{s}_\mathrm{IIP} &= \begin{pmatrix} u_{0,\mathrm{E}}\Delta\tau \\ u_{0,\mathrm{N}}\Delta\tau \\ 0 \end{pmatrix} + \begin{pmatrix} \tau\Delta u_{0,\mathrm{E}} \\ \tau\Delta u_{0,\mathrm{E}} \\ 0 \end{pmatrix} \\ &= \begin{pmatrix} u_{0,\mathrm{E}}\tau \\ u_{0,\mathrm{N}}\tau \\ 0 \end{pmatrix} \left(\frac{u_{0,\mathrm{up}}}{u_\mathrm{imp}} + 1\right)\left(\frac{\Delta u}{u}\right) \end{aligned} \tag{31}$$

of the predicted impact point in the local horizontal system.

The accumulated velocity change is obtained from an integration of the differential equation (27) along the ascent trajectory using the exponential density model (26) and the simplifying assumption of a constant flight path angle $\gamma = \arcsin(u_{\mathrm{up}}/u)$. For convenience, we substitute the altitude h as independent variable, which results in the differential equation

$$\frac{\mathrm{d}u(h)}{\mathrm{d}h} = \frac{\mathrm{d}u}{\mathrm{d}t}\frac{\mathrm{d}t}{\mathrm{d}h} = -\left(\frac{\rho}{2\beta}\right)u^2 \cdot \frac{1}{u\sin\gamma} = -\left(\frac{\rho_0 \mathrm{e}^{-h/H}}{2\beta\sin\gamma}\right)u(h). \tag{32}$$

Integration from the instantaneous altitude h_0 to infinity then yields the expression

$$\ln(u)\big|_{h_0}^{\infty} = H\left(\frac{\rho_0}{2\beta\sin\gamma}\right)\mathrm{e}^{-h/H}\Big|_{h_0}^{\infty} \tag{33}$$

or

$$\frac{\Delta u}{u} = \exp\left(\frac{H\rho_0 \mathrm{e}^{-h_0/H}}{2\beta\sin\gamma}\right) - 1 \tag{34}$$

for the accumulated velocity change due to atmospheric drag during the ascent of a sounding rocket.

For comparison, the predicted impact point distance from the launch site is shown in Fig. 5 for the early stage of the Test Maxus-4 mission. The data have been obtained from a numerical trajectory integration with and without drag as well as the linearized IIP model with supplementary drag correction. Depending on the epoch time for which the IIP computations were performed, ballistic coefficients between 30000 kg m^{-2} and 7000 kg m^{-2} have been assumed (cf. Table 5) to roughly account for the changing mass and aerodynamic properties of the rocket during the burn phase.

Evidently, consideration of the atmospheric drag on the ascent trajectory well avoids the overshooting of the impact point prediction near the end of the boost phase and yields consistent IIP location from burn-out onwards. During the early boost phase peak differences of about 7 km are obtained between drag-free IIP predictions and the numerical modeling of atmospheric perturbations which must be adequately considered in the range safety analysis. Basically, drag will always keep the actual impact point closer to the launch site than predicted by a purely Keplerian model. Thus a specified minimum distance of the impact point for a safe abort of the powered flight is only achieved at a later time than expected from drag free IIP predictions. In case of the Test Maxus-4 flight, the impact point distance from the launcher exceeds a value of 20 km from $t = 10$ s, whereas the drag free IIP prediction reaches this limit already at $t = 5$ s.

IIP predictions made with the linearized drag correction of Eqs. (31) and (34) compare well with the numerical trajectory model provided that the same ballistic coefficients are assumed. This is particularly surprising for the very early boost phase, where the impact trajectory remains well within the troposphere or lower stratosphere and the inherent assumptions of a constant flight path angle, a near

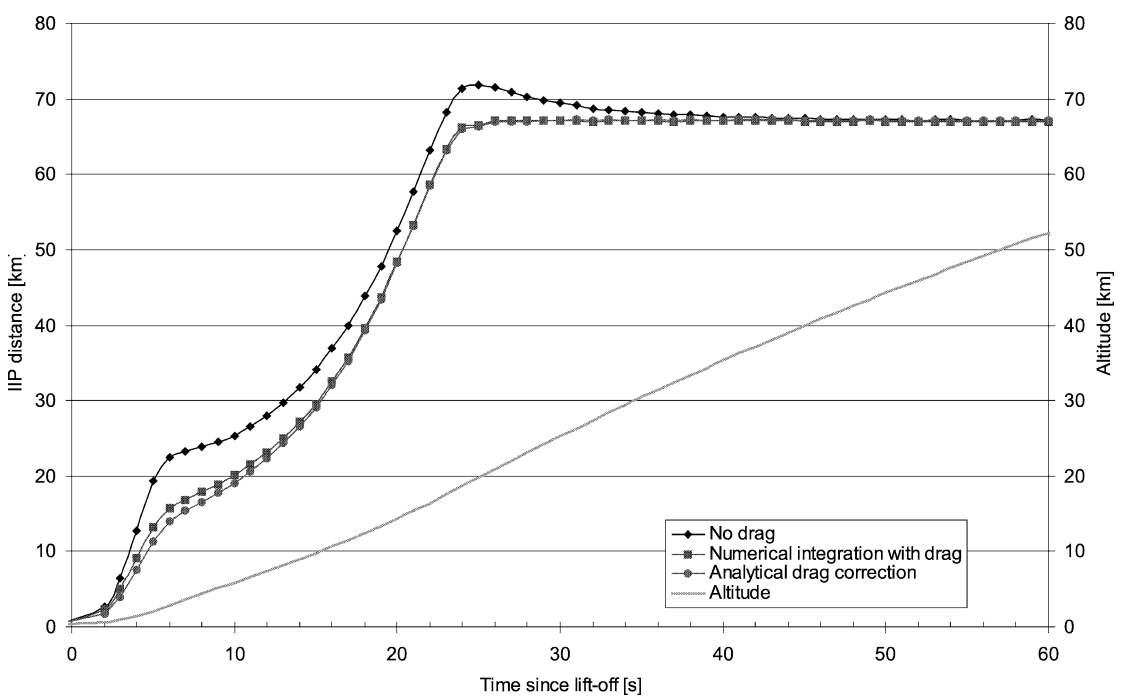

Fig. 5. Distance of the instantaneous impact point of the Test Maxus-4 rocket from the launch site as predicted by (a) a drag free model (diamonds), (b) a numerical trajectory integration with drag (squares) and (c) the linearized IIP model with drag correction (circles). A variable ballistic coefficient ranging from 30000 kg m^{-2} at lift-off to 7000 kg m^{-2} at burn end has been assumed for the combined motor and payload. For reference the altitude is shown on the right hand scale using a solid gray line.

Table 5
Ballistic coefficients assumed in the modeling of drag effects for Test Maxus-4 IIP predictions. Linear interpolation between the given grid points has been used to obtain intermediate values

Time since lift-off	
0 s	30 000 [kg m^{-2}]
5 s	18 000 [kg m^{-2}]
20 s	15 000 [kg m^{-2}]
$\geqslant$ 25 s	7000 [kg m^{-2}]

impulsive action of the atmospheric drag and a passage through the entire atmosphere are certainly violated. Despite these limitations, the derived equations cannot only provide useful rule-of-thumb estimates for the achievable accuracy of purely Keplerian IIP predictions but can also be used to improve drag free IIP computations if adequate a priori data on the ballistic coefficient of the launch vehicle are available.

5. Summary and conclusions

An IIP prediction model has been established, which is based on a plane-Earth parabolic trajectory model with first order corrections for surface curvature, gravity variation and Earth rotation. The model is less complex than a perturbed Keplerian trajectory model in inertial coordinates and thus well suitable for real-time computations. Yet, its agreement with the full modeling of conservative forces is high enough to introduce IIP prediction errors of less than 1.5% of the ground range for sounding rockets reaching altitudes of up to 700 km and flight times of about 15 min.

Complementary to the purely gravitational IIP prediction, a simplified model has been developed to assess the impact point offset due to atmospheric drag. While the model is restricted to the ascent phase of a mission and relies fully on an a priori knowledge of the ballistic coefficient, even a numerical trajectory integration using a canon-ball drag model is unable to account for the observed IIP excursions during the reentry and final descent. The latter perturbations must, therefore, be considered as unpredictable in a real-time computation of the instantaneous impact point. As such, the atmosphere poses a natural limit to the achievable IIP accuracy and adequate tolerances have to be incorporated into range safety procedures making use of instantaneous impact point predictions. This affects both the early flight phase, where a certain minimum distance of the IIP from the launch site must be achieved as well as the final reentry. Here atmospheric perturbations even larger than observed in the presented test cases may occur depending on the actual angle of attack at the reentry point.

Given the high inherent accuracy of GPS position and velocity measurements, which amounts to roughly 10 m and 1 m/s, tracking errors change the predicted IIP by less than 1 km and, therefore, contribute little to the overall error budget. On the other hand, the output rate supported by the GPS receiver provides a natural limit to the resolution of the IIP predictions. Assuming, for simplicity, a linear motion of the IIP during the thrust phase, the time between subsequent GPS navigation solutions should not exceed 1% of the boost duration to limit the intermediate IIP change to less then 1% of the total ground range. While this can usually be accomplished with the 1–10 Hz update rate of common receivers, it must be kept in mind that similar considerations apply for the accumulated data latency and end-to-end processing delays of the IIP prediction system. Here, a simple bottleneck may well invalidate the benefit of a high-performance GPS receiver.

Using the IIP model derived in the present study, an implementation inside a GPS receiver is at hand and has been performed within an experimental version of DLR's GPS Orion receiver (cf. [8]). While the output rate is presently limited to 2 Hz, the system demonstrates the basic concept of onboard IIP prediction and paves the way for future GPS based autonomous flight termination systems.

Acknowledgements

The present study makes use of GPS navigation data obtained during the Test Maxus-4 and the Maxus-4 campaigns. The authors are grateful to NASA/WFF and Kayser-Threde GmbH for providing their flight data sets for the purpose of this analysis.

References

[1] B. Bull, A real time differential GPS tracking system for NASA sounding rockets, in: Proceedings of the ION GPS-2000, Salt Lake City, Utah, 2000.
[2] B. Bull, J. Diehl, O. Montenbruck, M. Markgraf, Flight performance valuation of three GPS receivers for sounding rocket tracking, in: ION National Meeting 2002, 28–30 January 2002, San Diego, 2002.
[3] J. Diehl, Post-flight data analysis report for PTO P113E, NSROC Documentation #NSROC-01-00459; NSRCO Program Office, Wallops Island, Virginia, 16 March 2001.
[4] B. Hofmann-Wellenhof, H. Lichtenegger, J. Collins, Global Positioning System Theory and Applications, 4th ed., Springer-Verlag, Wien, New York, 1997.
[5] H.H. Koelle (Ed.), Handbook of Astronautical Engineering, McGraw-Hill, New York, 1961.
[6] L.D. Landau, E.M. Lifshitz, Course of Theoretical Physics, Vol. 1 Mechanics, 3rd ed., Butterworth-Heinemann, 1976.
[7] M. Markgraf, O. Montenbruck, GPS based analysis of DLR MPS36 radar tracking accuracy, DLR-GSOC TN 01-05 Deutsches Zentrum für Luft- und Raumfahrt, Oberpfaffenhofen, 2001.
[8] M. Markgraf, O. Montenbruck, F. Hassenpflug, P. Turner, B. Bull, A low cost GPS system for real-time tracking of sounding rockets, in: Proc. 15th European Symposium on European Rocket and Balloon Programmes and Related Research, Biarritz, 2001.
[9] O. Montenbruck, E. Gill, Satellite Orbits, Springer-Verlag, Heidelberg, 2000.

[10] O. Montenbruck, M. Markgraf, Maxus-4 Orion GPS tracking system flight report, MAX4-DLR-RP-0001 DLR/GSOC, Oberpfaffenhofen, 2001.
[11] H. Moritz, Geodetic Reference System 1980, Bulletin Géodésique, The Geodesists Handbook, International Union of Geodesy and Geophysics, 1988.
[12] NRC, Streamlining Space Launch Range Safety, National Research Council, Aeronautics and Space Engineering Board, National Academic Press, Washington, 2000.
[13] F.J. Regan, S.M. Anandakrishnan, Dynamics of Atmospheric Re-Entry, AIAA Education Series, American Institute of Aeronautics and Astronautics, Washington, DC, 1993.
[14] B.B. Willemse, Information on the VS40 sounding rocket, Technical University Delft, 1997, http://dutlls1.lr.tudelft.nl/oshelp/projects/r1/vs40.html.